

RSC Advances

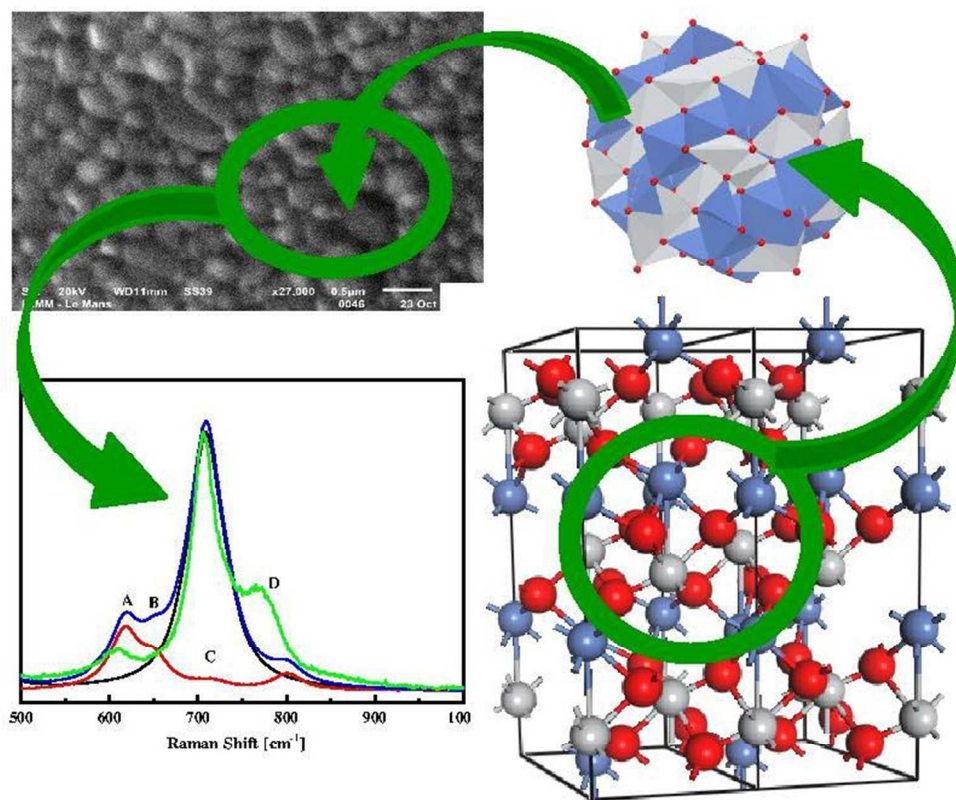


This is an *Accepted Manuscript*, which has been through the Royal Society of Chemistry peer review process and has been accepted for publication.

Accepted Manuscripts are published online shortly after acceptance, before technical editing, formatting and proof reading. Using this free service, authors can make their results available to the community, in citable form, before we publish the edited article. This *Accepted Manuscript* will be replaced by the edited, formatted and paginated article as soon as this is available.

You can find more information about *Accepted Manuscripts* in the [Information for Authors](#).

Please note that technical editing may introduce minor changes to the text and/or graphics, which may alter content. The journal's standard [Terms & Conditions](#) and the [Ethical guidelines](#) still apply. In no event shall the Royal Society of Chemistry be held responsible for any errors or omissions in this *Accepted Manuscript* or any consequences arising from the use of any information it contains.



140x122mm (150 x 150 DPI)

Vibrational and electronic peculiarities of NiTiO₃ nanostructures inferred from first principle calculations

Cite this: DOI: 10.1039/x0xx00000x

Received 00th January 2012,
Accepted 00th January 2012

DOI: 10.1039/x0xx00000x

www.rsc.org/

M. A. Ruiz Preciado,^{a,b,c} A. Kassiba,^b A. Morales-Acevedo^c and M. Makowska-Janusik^{a†}

Structural, electronic and vibrational properties of nanostructured (NiTiO₃)_n clusters were calculated by numerical models based on DFT and semi-empirical quantum chemistry codes. The clusters were built by using initial atomic positions of crystalline ilmenite which were relaxed to ensure stable and energetically favourable geometries. For the electronic properties, the semi-empirical PM6 parameterisation method was used to evaluate the HOMO-LUMO energy differences versus nanocrystal sizes. The quantum confinement effect was traduced on the electronic features with the cluster size reduction. Theoretical UV-vis absorption as well as the Raman spectra show drastic influence of surface on the electronic and the vibrational properties of nanoclusters. Theoretically it was proved that the powder NiTiO₃ exhibits patchwork of the properties of bulk ilmenite material, amorphous Ni-Ti-O structures and atoms located at the surface of the investigated cluster.

Introduction

Photocatalytic processes have been intensively discussed and investigated in the last two decades due to their potential applications to solve problems of waste from the environment or alternatively to create new sources of energies¹⁻². As examples it can be mentioned that the photocatalytic reactions contribute to remediation of environmental pollution by degradation of organic organisms or to production of hydrogen from water dissociation for renewable energies³⁻⁹. The considered processes are based on photoinduced charge transfers caused by light sources (visible or UV) in the semiconducting oxides.

Beyond application in photovoltaic devices, the titanium dioxide (TiO₂) is one of the most efficient material to monitor photocatalytic reactions and possesses the best performances associated with good stability, versatile applications, non-toxicity and low cost¹⁰⁻¹². Photocatalytic reactions based on TiO₂ under UV irradiation were carried out to clean waste water from different types of impurities¹³⁻¹⁶. The kinetics of reactions is characterized by short relaxation times to achieve complete removal of pollutants. However, the need of UV to induce the required charge transfer in mentioned reactions limits the performances of TiO₂ and therefore photocatalytic materials under visible light irradiation are worth of interest since solar light spectrum can be exploited on large scale to activate high photocatalytic reactions.

The perovskite-type oxides, such as tantalates and titanates, have recently attracted much attention, because of their high photocatalytic activities under UV irradiation and, more remarkable, under visible light¹⁷⁻¹⁹. These titanates such as ATiO₃ (A = Ca, Bi, Pb, Fe, Co, Mn, Ni, Cu, and Zn) have been studied as functional inorganic materials with wide applications as electrodes for solid oxide fuel cells, metal-air barriers, gas sensors, solid lubricants, and high-performance catalysts²⁰⁻²². Among these materials, we consider the transition metal titanates such as FeTiO₃, CoTiO₃, MnTiO₃, NiTiO₃, etc. that crystallize in the ilmenite structure at atmospheric pressure²³⁻²⁶. They are of particular interest due to their versatile electrical and magnetic properties such as the antiferromagnetic behavior^{27,28}. The related properties of several titanate oxides have been investigated experimentally and theoretically. FeTiO₃ is worthy of interest as natural mineral and a major source of titanium for the commercial production of TiO₂. The electronic, magnetic, structural and elastic properties for the bulk FeTiO₃ have been computed using density functional theory (DFT) formalism and *ab-initio* calculations²³⁻²⁵. Within such approaches, the electronic ground-state properties as well as charge-transfer involved in FeTiO₃ were determined by a strong coupling of the structure with charge distribution. The quantum-mechanical description of these features is very sensitive to the treatment of electronic exchange and correlation energies. This allows concluding that the metal titanates are strongly correlated systems and therefore the electron correlation part should be treated adequately.

Table 1 Lattice parameters and atomic fractional coordinates of NiTiO₃ crystal structures

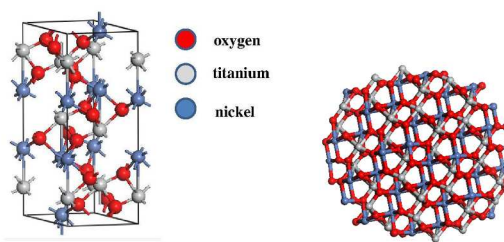
Atoms name	x/a	y/b	z/c
Ni	0	0	0.3499(1)
Ti	0	0	0.1441(1)
O	0.3263(7)	0.0214(10)	0.2430(3)
Cell parameters	a = b = 5.0289(1) Å c = 13.7954(2) Å α = β = 90° γ = 120°		
Space group	R $\bar{3}$ (No. 148)		

The present work reports theoretical approaches to model nanostructures and simulate the electronic and vibrational properties of NiTiO₃ nanoclusters. Comparative studies were performed by using also bulk crystal with its infinite and periodic structure. Previous theoretical approaches developed by Xin et al.²⁹ were used to compute the electronic properties of bulk and infinite NiTiO₃ system. However, to our best knowledge no particular models have been performed to compute and predict the physical properties of the NiTiO₃ nanostructures. The study of nanosized systems is of great interest with regard to the critical role of the specific active surface in physical phenomena. Particularly, interfaces between the active material and the surrounding media contribute critically to the efficiency of heterogeneous catalysis. However, theoretical modeling and numerical simulations to predict electronic, optical, structural, vibrational and related properties of nanoparticles are challenging tasks. The numerical approach presented here was partially conducted in our former works devoted to functional semiconducting systems³⁰⁻³². The nanostructures were built from their native bulk crystals with specified atomic positions as involved in defined space groups. Also in this work, modeling of bulk systems is of primary importance to settle the methodology for the structural, vibrational and electronic properties of nanostructures. The quantum chemical calculations were based on first-principles calculations using ultrasoft pseudopotential of the plane-wave within the DFT formalism. The generalized gradient approximation extended by Hubbard parameters was used to evaluate the electronic properties of NiTiO₃ bulk crystal.

The original task of this work consists in the implementation of the crystal structure at nanoscale including relaxation of the outermost surface atoms with their suitable treatment. The changes on their electronic and vibrational properties were accurately described as function of the structural features of the investigated nanoclusters. Also the surface influence was demonstrated on the physical properties of the clusters. The simulation of electronic band structures clarifies the charge transfer characteristics. This approach paves the way to the mechanisms behind the photocatalytic activity of the nanosized NiTiO₃ materials. The theoretical results are compared to the data obtained by experimental investigations of the relevant features of NiTiO₃ nanostructures.

Computational details and cluster building methodology

The crystal structures were computed for two different configurations of the material. One of them was considered like bulk NiTiO₃ monocrystal crystallized in the ilmenite phase; i.e. space group R $\bar{3}$ (No. 148)³³. The second was chosen as nanocrystalline cluster with different sizes possessing the ilmenite structure in the core. Therefore, the unit cell of ilmenite NiTiO₃ was built using the cell parameters $a = b$

**Figure 1** The unit cell of crystal NiTiO₃ (left) and the unpassivated nanocrystalline made by the formulae (NiTiO₃)₈₂ (right)

= 5.0289 Å, $c = 13.7954$ Å and the angular parameters $\alpha = \beta = 90^\circ$ and $\gamma = 120^\circ$. The positions of representative atoms within the unit cell are summarized in Table 1. The crystal structure of NiTiO₃ was built using the Materials Studio Program Package. The same simulation software was used to build the (NiTiO₃)_n nanostructures with diameters from 0.6 nm up to 2.6 nm associated to clusters composed by (NiTiO₃)₂ and (NiTiO₃)₁₈₃ units, respectively. Consequently, all the investigated nanocrystal exhibit spherical shape and stoichiometric composition. According to our previous work on other class of nanocrystalline systems, dangling bonds were not specially saturated³¹. The unit cell of monocrystal and the morphology of (NiTiO₃)₈₂ cluster are depicted in Figure 1.

The electronic properties of NiTiO₃ single crystal were calculated using the DFT methodology. The quantum chemical calculations were performed using the Cambridge Serial Total Energy Package (CASTEP)³⁴; i.e. the module of the Materials Studio Program. The CASTEP is based on the evaluation and analysis of the total energy inferred from plane-wave pseudopotential method. The first task deals with the geometry optimisation of the investigated crystal structure which is built and evaluated with respect to the total energy minimization within the Broyden-Fletcher-Goldfarb-Shanno (BFGS) algorithm³⁵. During the geometry optimisation procedure, the symmetry of the structure was frozen but the size of unit cell was allowed to change. The convergence criteria for optimization procedure were chosen as hereafter outlined. The convergence of the total energy during the geometry optimization procedure cannot be greater than $2 \cdot 10^{-5}$ eV/atom, the force on the atom must be less than 0.01 eV/Å, the stress on the atom less than 0.02 GPa and the maximal atomic displacement no more than $5 \cdot 10^{-4}$ Å. The electron exchange-correlation energy was treated within the framework of the generalized gradient approximation (GGA) using Perdew-Burke-Ernzerhof (PBE)³⁶ potential. To accelerate the computational runs, the ultrasoft pseudopotential formalism was used. In this frame, calculations were performed for Ti ($3d^2 4s^2$), Ni ($3d^8 4s^2$) and O ($2s^2 2p^4$) electrons. The cut-off energy of the plane-wave basis set was chosen to be equal to 500 eV. The integration by numerical sampling for specific directions over the Brillouin zone (BZ) were carried out using the Monkhorst-Pack method with a $8 \times 8 \times 8$ special k -point mesh. The total energy convergence criterion was assumed to be fulfilled when the self-consistent field (SCF) tolerance; i.e. equal to 10^{-5} eV/atom.

The electronic properties of the NiTiO₃ crystal were computed using the above mentioned parameters as specified for the geometry optimization procedure. The calculations were carried out in spin restricted as well as spin unrestricted procedures applying GGA/PBE potential and Heyd-Scuseria-Ernzerhof (HSE06) range-separated hybrid functional^{37,38}. Hummer et al.³⁹ show that the HSE06 functional yields the correct

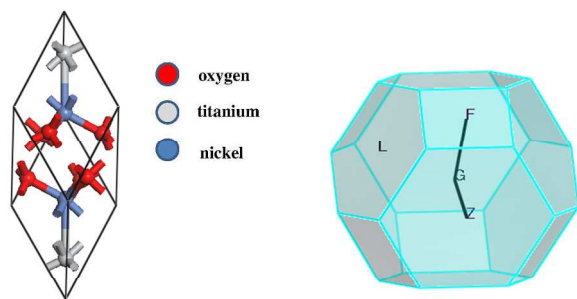


Figure 2 Primitive unit cell of NiTiO₃ (left) and the corresponding reciprocal lattice (right) with the coordinates of the special points of the BZ: F (1/2, 1/2, 0); Γ (0, 0, 0); K (1/4, 1/4, 1/4) and Z (1/2, 1/2, 1/2)

electronic band structure for the semiconductors of group-IV. Also the work of Śpiewak et al.⁴⁰ shows that the HSE06 potential may reproduce better the electronic properties of defected Ge single crystal. Contrary to this, other works underline that the range-separated functionals show improvement for strong charge transfer systems^{41,42}. It is generally known that classical DFT potentials does not reproduce correctly far-nucleus asymptotic behaviour^{43,44} and underestimates the excitation energies notably for charge-transfer processes⁴⁵. The range-separated potentials lead to the partitioning of the total exchange energy into short-range and long-range contributions:

$$E_X = E_X^{sr} + E_X^{lr} \quad (1)$$

To improve the exchange functional for calculating the long-range electron–electron interaction by the HF exchange integral, the standard error function is used. The repulsion electron operator is also divided into short-range and long-range part and can be defined for two electron at the r_{ij} distance as:

$$\frac{1}{r_{ij}} = \frac{1 - [\alpha + \beta \text{erf}(\mu r_{ij})]}{r_{ij}} + \frac{\alpha + \beta \text{erf}(\mu r_{ij})}{r_{ij}} \quad (2)$$

where α and β parameters define the exact exchange percentage between short and long-range exchange functional. μ represents the weighting factor which controls the separation between short-range exchange functional and the long-range part of HF exchange integral.

The Kohn–Sham equation was also solved using the GGA/PBE functional extended by the Hubbard parameters. The introduced methodology contributes to precise insights on the electronic properties of material. The major drawback of all functionals lies in the underestimation of the calculated electronic band gap⁴⁶. This is frequently encountered due to the approximate calculations of the electron self-interaction energies. Also pure local density approximations (LDA)⁴⁷, the generalized gradient approximations (GGA)⁴⁸ and even the hybrid functionals^{49–51} can suffer from some lacks of precision for so called "strongly correlated" systems.

One relevant solution to describe correlated electrons in solids concerns the Hubbard model⁵² based on extended LDA approach also referred as LDA+U. It decreases the electron self-interaction error by selective adding an energy correction to localized electron states as for d or f orbitals where the self-interaction is particularly large. To construct an appropriate functional, the LDA+U approach subdivides the charge density into two subsystems with delocalized and localized features. In the multiband Hubbard model the effective LDA+U energy functional is written as:

$$E_{LDA+U} = E_{LDA} + E_{HF}(n_{\mu\nu}) - E_{dc}(n_{\mu\nu}) \quad (3)$$

where E_{LDA} denotes standard LDA energy functional, E_{HF} is the Hartree-Fock (HF) functional, the E_{dc} is the double counting term and $n_{\mu\nu}$ is one particle density matrix. The HF part can be written as follows:

$$E_{HF}(n_{\mu\nu}) = \frac{1}{2} \sum (U_{1324} - U_{1342}) n_{12} n_{34} \quad (4)$$

Where the U_{1324} terms represent the renormalized Coulomb integrals. In the LDA+U approach, the Kohn-Sham equation is supplemented by the non-local potential. From the other side, the DFT/Hubbard method fails to compute the correct energy difference between systems with localized/correlated and delocalized/uncorrelated electronic states⁵³. In such approach, the LDA/GGA+U methodology was successfully applied to compute the electronic properties of different ternary oxides such as CuAlO₂⁵⁴, CuAl₂O₄⁵⁵, Pr₂Ti₂O₇ or Ce₂Ti₂O₇⁵⁶, MnFe₂O₄⁵⁷. Based on the outlined theoretical framework, the influence of the Hubbard parameter U on the electronic properties of NiTiO₃ was investigated on the crystalline structure in bulk material or in nanosized clusters taking into account the strong correlation of the d -orbital electrons.

In the present work, the electronic properties of the (NiTiO₃)_n nanoclusters were also calculated. Up to our knowledge it is first time that nickel titanates nanostructures were studied theoretically. The methodology requires two different calculations codes able to perform the simulations and also to ensure their stability. Thus, Gaussian09 and MOPAC (Molecular Orbital PACKage)⁵⁸ quantum chemistry programs were used. With regard to the size of investigated clusters the semiempirical single point calculations were performed applying parameterized self-consistent restricted HF (SCF RHF) PM6 method⁵⁹. The convergence of the SCF procedure was achieved with energy uncertainty not greater than 10⁻⁶ hartree and no more than 150 required iterations. Within such approaches, the electronic properties of two different clusters families were computed. The first one deals with (NiTiO₃)_n clusters possessing ilmenite crystal structure without any reconstruction. The second consider the same clusters like specified previously but their geometry was optimised according to the total energy minimization. The geometry of all clusters was specified in cartesian coordinates with C1 symmetry. The gradient convergence tolerance was equal to 10⁻⁶ hartree/bohr using the quadratic approximation (QA) method^{60–62} updating the Hessian matrix during the optimization. The Hessian evaluation was performed to exclude the structures giving rise to negative modes.

Results and discussion

Structure and electronic properties of bulk ilmenite NiTiO₃

The GGA/PBE functional was used to build stable NiTiO₃ crystal geometry and to calculate the related physical responses. In a first step, the geometry optimization of the crystal structure was performed. The changes on the optimised atomic distances were less than 5% compared to the starting values from defined crystallographic data. It is in agreement with former report by Xin et al.²⁹. The noticed departures could be attributed to the fact that the present calculations works at T = 0 K, whereas the experimental structural data measurements are performed generally at room temperature. Thus, the relatively low deviation between optimized values and experimental structural data indicates that GGA/PBE is relevant computational functional to describe the structures of the NiTiO₃ crystal. Following the performed geometry optimization one may conclude that ilmenite NiTiO₃ structure appears as layered

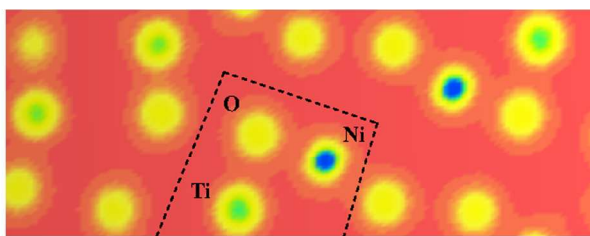


Figure 3 Electron density projection in selected plane of NiTiO₃ ilmenite structure

organisation depicted in Fig. 2 (panel left), where Ti and Ni atoms form the layers separated by oxygen atoms.

The electronic properties of NiTiO₃ crystal were computed within the spin polarized approach for a primitive unit cell (see Fig. 2). The band structure calculations were performed in *k* space within the BZ directions shown in Fig. 2 (right panel). The DFT/HSE06 functional gives unsatisfactory results. The obtained energy gap is equal to 1.23 eV whereas the experimental data are within 2.12 eV – 2.18 eV⁶³⁻⁶⁵. Also the DFT/PBE functional without and within the Hubbard approximation was considered. The mentioned functional without Hubbard approximation and in spin polarized regime gives the energy gap of NiTiO₃ crystal equal to 0.77 eV. This shows that nonempirically tuned range-separated DFT methods cause a significant improvement over traditional GGA functional but does not give good results for the studied crystal. The large discrepancies suggest the presence of strongly correlated electrons from the nature of the considered (Ti, Ni) ions leading to the necessity to explore the Hubbard approximation in such systems. Within the approach based on DFT/PBE potential, the electron density depicted in Fig. 3 informs also on the covalent character of the O-Ti, O-Ni and Ti-Ni bonds. This behavior supports the nature of strongly correlated system and the necessary evolution of the theoretical functional to conciliate the predictive electronic features with the experiments.

The functional modified by the Hubbard approximation uses parameters which can be adequately chosen for Ti 3d and Ni 3d valence electrons in order to evaluate the energy band gap values. The relevance of the chosen Hubbard parameters *U* for obtained band gaps is demonstrated from the summary in Table 2. The correct evaluation of electronic behaviour in agreement with experiment requires fixed Hubbard parameters at 3.5 eV and 4.5 eV for Ti 3d and Ni 3d electrons, respectively. Thus,

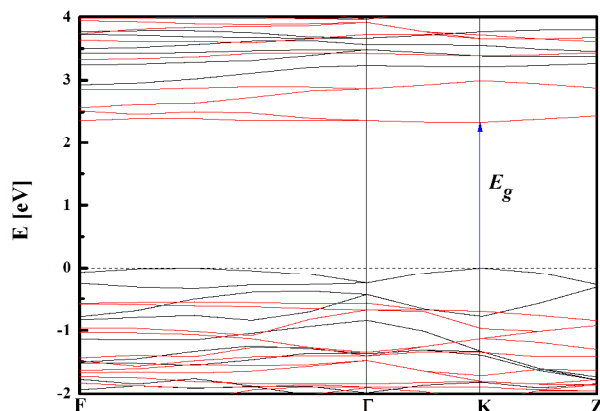


Figure 4 Electron band structure calculated by DFT/PBE functional within Hubbard approximation *U*. The energy levels with spin polarized alpha electrons (black) and energy levels with beta state (red) are shown

Table 2 Hubbard *U* parameter values for the Ti d and Ni d orbitals and the energy gap value calculated by DFT/PBE+*U* methodology

Ti 3d	Ni 3d	E_g [eV]
0	0	0.77
2.5	2.5	1.75
3.5	4.5	2.33
4.5	3.5	1.94
4.5	4.5	2.46

DFT/PBE+*U* method may provide a satisfactory qualitative electronic structure calculation with adequate choice of the Hubbard parameters. The electronic band structure computed with the $U_{Ti}=3.5$ eV and $U_{Ni}=4.5$ eV is presented in Fig. 4. This plot infers that NiTiO₃ structure exhibits direct semiconducting nature with energy gap equal to 2.33 eV. The spin polarized character is also included in the predictive electronic features. Thus, the top of valence band is built by spin polarized alpha

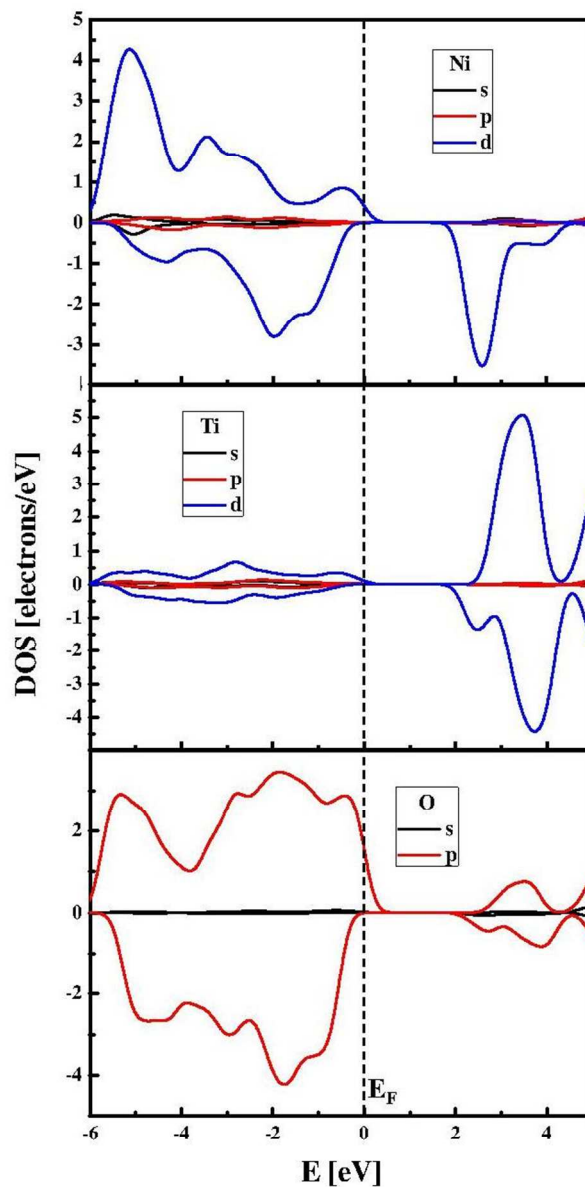


Figure 5 Electron density of state (DOS) calculated for NiTiO₃ ilmenite structure by using DFT/PBE functional augmented by Hubbard approximation: polarized alpha electrons (top) and beta electrons (bottom)

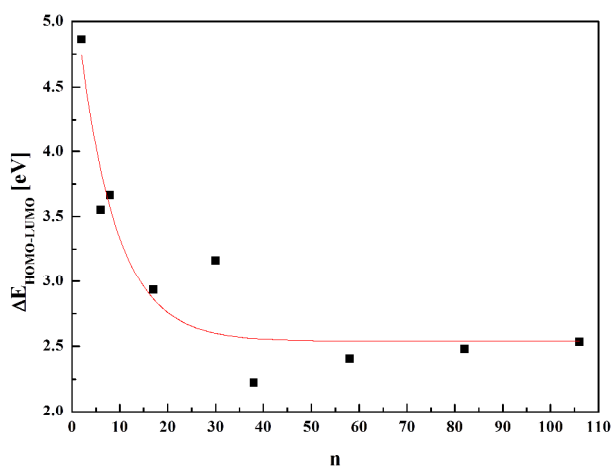


Figure 6 Evaluation of the $\Delta E_{\text{HOMO-LUMO}}$ energy splitting versus number n of $(\text{NiTiO}_3)_n$ units calculated by PM6 methodology

electrons while the bottom of conduction band is composed by beta state. In addition, the partial density of states depicted in Fig. 5, points out that the spin polarized alpha electrons with energies at the top of the valence band are emanating from hybridization of Ni 3d and O 2p electrons; while hybridization of the Ti 3d and Ni 3d states define the electronic structure at the bottom of conduction band in agreement with former work of Salvador et. al.⁶⁶.

The energy dispersion of the electronic states allows to calculate the effective masses of charge carriers. The diagonal elements of the effective mass tensor for electrons and holes are calculated as the energy derivatives around K point of BZ following the equations:

$$\frac{1}{m_{eij}^*} = \frac{1}{\hbar^2} \frac{\partial^2 E_c(k)}{\partial k_i \partial k_j} \quad \text{and} \quad \frac{1}{m_{hij}^*} = \frac{1}{\hbar^2} \frac{\partial^2 E_v(k)}{\partial k_i \partial k_j} \quad (5)$$

The effective mass of electrons and holes is determined by fitting the conduction and valence band (see Fig. 4), respectively, to parabolic functions. One may see that the top of valence band and bottom of conduction band are symmetric around K point of BZ. In this case the calculated electrons and holes effective masses are equal to $m_e^* = 2.0986 \cdot m_e$ and $m_h^* = 0.6836 \cdot m_e$ with the same values in both K - Z and K - Γ directions of BZ. The relatively high values of reported parameters suggest that the mobility of charges in investigated NiTiO_3 single crystal is relatively low. This result is of particular importance for the very low electrical conductivity (10^{-9} S/m) achieved in NiTiO_3 at moderate temperatures up to 200°C ⁶⁷. The performed calculations confirm that in the studied material its electrical conduction observed at temperature below 700 K seems to be extrinsic type, governed by impurities, interstitials, etc. It takes place via the small polaron hopping mechanism⁶⁴.

Nanocrystalline ilmenite NiTiO_3 clusters

Structural and electronic features

Structural and electronic properties of NiTiO_3 nanocrystals were investigated for nanoparticles built from the ilmenite bulk material. The investigated nanostructures possess spherical shape with variable number of $(\text{NiTiO}_3)_n$ units from $n=2$ up to 183. The single point DFT/PBE and DFT/HSE06 calculations were performed for clusters with n from 2 up to 20 but the results did not show correct behaviour of the energy difference

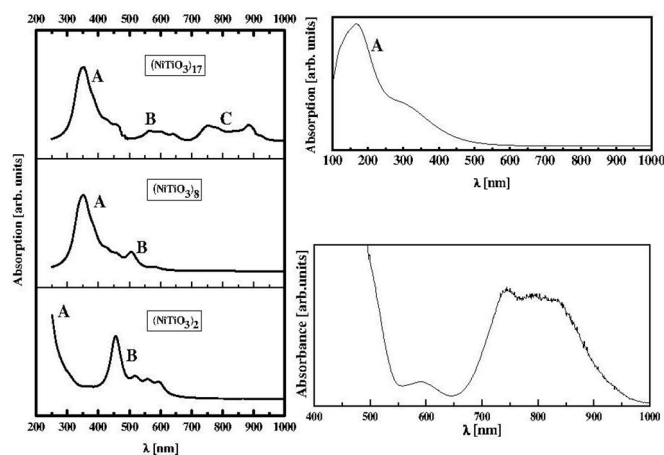


Figure 7 UV-Vis absorption spectra calculated by the PM6 model for different clusters (left panel), calculated spectrum for bulk crystal by using DFT/PBE+U functional (top right panel) and the experimentally obtained data (bottom right panel)

between the highest unoccupied molecular orbital (HOMO) and lowest unoccupied molecular orbital (LUMO) versus the size of the cluster. It is known that the standard DFT scheme is not useful for finite-sized objects because the asymptotic potential, absent in a bulk, plays a crucial role in cluster energy by addition and removal of electrons. This leads to calculated energy gaps for finite-sized objects often much smaller than the real gap⁶⁸.

Contrary to the results obtained by DFT, the PM6 semi-empirical methodology was successfully applied for such clusters leading to correct estimation of the energy gap in nanosized NiTiO_3 . In Fig. 6, the computed energy differences $\Delta E_{\text{HOMO-LUMO}}$ versus the cluster sizes are depicted. The reported energy gap splitting as function of the $(\text{NiTiO}_3)_n$ units demonstrates the size induced quantum confinement effect. This is in agreement with the experimental report⁶⁹ on NiTiO_3 nanoparticles which give rise to blue shift of the absorption spectra compared to the bulk material. The $\Delta E_{\text{HOMO-LUMO}}$ reaches the saturated value for the clusters built by $n \geq 50$ for $(\text{NiTiO}_3)_n$ units. The energy gap value for the large sized clusters saturates at 2.55 eV.

Using the PM6 model, UV-Vis absorption spectra were computed for selected clusters, namely $(\text{NiTiO}_3)_2$, $(\text{NiTiO}_3)_8$ and $(\text{NiTiO}_3)_{17}$. Large sized clusters were not considered due the computer system memory limitation. The calculated spectra are summarized in Fig. 7 along with the experimental data. A good agreement is demonstrated between the spectrum calculated by PM6 model for $(\text{NiTiO}_3)_{17}$ cluster and the measured one for crystalline powder of NiTiO_3 . Increasing the cluster diameter (the unit number $n=2$ -17), the position of A band (see Fig. 7 left panel) shifts to red spectral range. The band labelled B with well pronounced intensity for small clusters undergo red shift and decreased notably with increasing the cluster sizes. For the cluster $(\text{NiTiO}_3)_{17}$ with diameter 1.20 nm an additional broad peak C develops in the range 750-900 nm. The broad band in that spectral range was also demonstrated experimentally. The UV-Vis spectrum calculated for the bulk crystal NiTiO_3 by using DFT/PBE+U functional (see Fig.7, right-top panel) did not match with the experiment in the high wavelength range where C band is involved. It

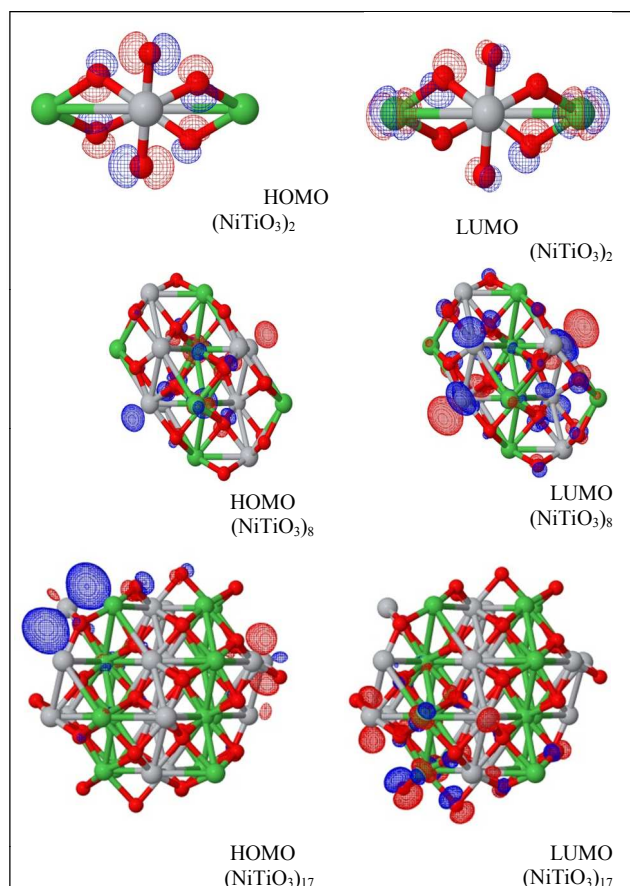


Figure 8 HOMO and LUMO orbitals calculated by PM6 model for $(\text{NiTiO}_3)_2$, $(\text{NiTiO}_3)_8$ and $(\text{NiTiO}_3)_{17}$ clusters

confirms that the surface effect in experimental absorption spectrum of the NiTiO_3 powders plays sensitive role.

The HOMO and LUMO orbitals, depicted in Fig. 8, for the investigated clusters $(\text{NiTiO}_3)_2$, $(\text{NiTiO}_3)_8$ and $(\text{NiTiO}_3)_{17}$, show their explicit separation and contribute to the low energy absorption spectra. The separation feature between HOMO and LUMO orbitals is not revealed for the bulk NiTiO_3 concerning top of valence band and bottom of conduction band. The observed details suggest that the separation of HOMO and LUMO orbitals gives rise to B and C bands.

The comparison of the theoretical and the experimental UV-Vis absorption spectrum performed for $(\text{NiTiO}_3)_{17}$ nanocluster clearly indicates interesting optical activity of the system in the UV and the visible range of solar spectrum. A broad absorption edge situated at ~ 410 nm is associated to $\text{O}^{2-} \rightarrow \text{Ti}^{4+}$ charge transfer transitions. The higher wavelength shoulder is associated to the crystal field splitting of NiTiO_3 , associated to the $\text{Ni}^{2+} \rightarrow \text{Ti}^{4+}$ transitions⁷⁰. Thus, the photoinduced charge transfers which are required for photocatalytic reactions may be ensured by several electronic transitions covering UV and visible light range involved for the nanosized NiTiO_3 . They contribute to the efficient photocatalytic activity. Finally, it is worth noting that the resolved details on the theoretical absorption spectra are induced by calculations performed without any temperature influence on the structural relaxation of NiTiO_3 clusters. A possibility to conciliate the shapes of absorption bands between theory and experiments may be realized through the electron-phonon interaction and the

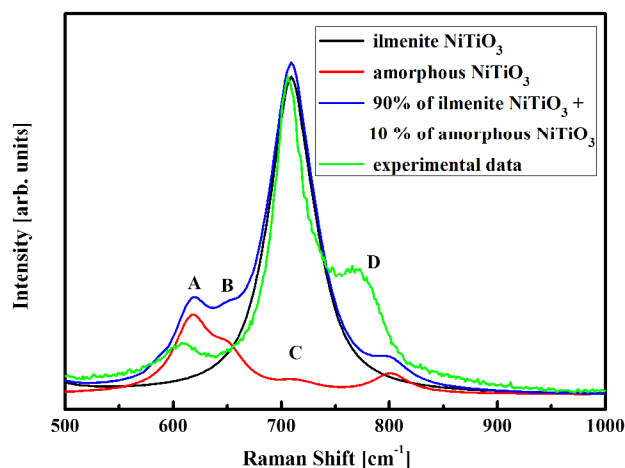


Figure 9 Raman shift for the $(\text{NiTiO}_3)_{17}$ nanoparticles calculated by the parametrised PM6 method as well as experimental spectrum

Franck-Condon rule for the optical transition probabilities as was conducted in our former work⁷¹.

Raman spectra of nanocrystalline NiTiO_3

Taking into account the effect of electron-phonon interaction, the evaluation of the Raman spectra related to the selected clusters were performed within the PM6 approach. The Raman spectra were calculated using standard procedure implemented in Gaussian program package. The calculations were performed on two $(\text{NiTiO}_3)_{17}$ clusters. The one where the ilmenite crystal structure was frozen and the other system possessing reconstructed surface by geometry optimization procedure according to the total energy minimization criterion. The last cluster is characterized by complete amorphous network. The experimental and calculated Raman spectra modeled for $(\text{NiTiO}_3)_{17}$ nanoclusters and for NiTiO_3 powder are depicted in Fig. 9.

For the cluster $(\text{NiTiO}_3)_{17}$ with rigorous ilmenite structure, the calculations show only a single mode at position C. The experimental Raman spectrum shows an intense band with wavenumber position in agreement with the calculated value. C band is also the most intense details in the experimental Raman spectrum. The titanates as NiTiO_3 , CoTiO_3 and Na_4TiO_4 possess hexacoordinated Ti–O–Ti groups and their Raman modes are associated to the main band located at 705, 688, 737 cm^{-1} , respectively⁷²⁻⁷⁴. Therefore, it was summarized that the Ti–O–Ti stretch mode should appear in the vicinity of 700 cm^{-1} . For NiTiO_3 the band at 720 cm^{-1} concerns the Ti-O-Ti vibration of crystal structure.

The Raman bands named A, B and D with relatively low intensity compared to C band, are consecutive to the full optimization and relaxation of the nanocluster structures. This procedure which leads to stable amorphous networks ensures the molecular bonding distortions including bond lengths and angles. Such structural changes modify the vibration features and, as shown from experimental and theoretical aspect, new Raman bands appear. A superposition of the main Raman band (90%) of stretching O-Ti-O and the secondary bands (10%) related to amorphous structure leads to the theoretical Raman spectrum which reproduces the features of the experimental one. The slight departures on the band positions may be explained by the fact that anharmonic vibration terms were not

considered in the calculation model. The main origin may be related to bond frequency distributions due to amorphization or the occurrence of vacancies or antisites contributing to the damping and frequency shifts of Raman modes^{75,76}. In this frame, it was proved that the bands located at 617 and 690 cm⁻¹ are inferred from stretching of Ti-O and bending of O-Ti-O bonds meanwhile the contribution at 547 cm⁻¹ result from Ni-O bonds⁶⁹.

As illustrated from the theoretical analysis and the experimental Raman investigations, the organization of the powder material is fully accounted by the carried out analysis. With such morphology, the particle core bring the signature of infinite and bulk crystal while the outermost particle surface account for the amorphization features. This fact is presumably the manifestation of surfaces states with relaxation and reconstruction of the outermost particle layers.

Conclusions

Electronic, optical and vibrational properties of (NiTiO₃)_n nanostructures were investigated and compared to bulk ilmenite NiTiO₃. The investigated nanostructures possess spherical shape with the number of (NiTiO₃)_n units modified from n=2 up to 183. The PM6 semi-empirical methodology was relevant to reproduce the valuable estimation of the energy gap in nanosized NiTiO₃ structures. The value of the ΔE_{HOMO-LUMO} saturates to 2.55 eV for the clusters built by n=50 and more (NiTiO₃)_n units. The UV-Vis absorption spectra were calculated using PM6 methodology for nanostructures and compared with experiments. The obtained spectra confirm that the surface effects in NiTiO₃ powders contribute by additional band edges. The comparison of the theoretical and the experimental UV-Vis absorption spectrum performed for (NiTiO₃)₁₇ nanocluster clearly indicates promising optical activity of the system in the UV and the visible range of solar spectrum. The NiTiO₃ nanoclusters exhibit also relevant properties as required for efficient photocatalysis.

The calculated Raman spectra for NiTiO₃ clusters show a noticeable contribution of the surface to the vibrational properties. Among the features of Raman spectra, those related to active modes of ilmenite structure and those inferred from amorphous NiTiO₃ can be distinguished. A theoretical superposition of a Raman band which bring 90% of band intensity associated to stretching O-Ti-O mode and secondary less intense bands (10%) related to amorphous structure accounts remarkably for the main features of the experimental spectrum.

Finally, the present work points out the relevant optical properties of NiTiO₃ clusters able to harvest visible light for efficient photocatalytic reactions. However, the low mobility of charges carriers demonstrated from effective mass estimation, remains open questions which can be solved by doping procedure. This is matter of current development.

Acknowledgements

Calculations have been carried out in Wroclaw Center for Networking and Supercomputing <<http://www.wcss.wroc.pl>> (Grant no. 171). The MATERIALS STUDIO package was used under POLAND COUNTRY-WIDE LICENSE. The authors acknowledge the financial support of Polonium program 31300 TA – 2014 for researchers mobility. Marco Ruiz acknowledges the doctoral school 3MPL for the financial support.

Notes and references

- ^a Institute of Physics, Jan Dlugosz University in Czestochowa, Al. Armii Krajowej 13/5, 42200 Czestochowa Poland.
- ^b Institute of Molecules and Materials of Le Mans, Université du Maine, 72085 Le Mans, France.
- ^c Centro de Investigación y Estudios Avanzados del IPN, Unidad Zacatenco, México.
- † corresponding author: m.makowska@ajd.czest.pl
- 1 L. Linsebigler, G. Lu and J. T. Yates Jr., *Chem. Rev.* 1995, **95**, 735.
- 2 K. Nakata and A. Fujishima, *J. Photochemistry and Photobiology C: Photochemistry Rev.* 2012, **13**, 169.
- 3 S. Bagwasi, B. Tian, J. Zhang and M. Nasir, *Chemical Engineering J.* 2013, **217**, 108.
- 4 C. L. Torres-Martinez, R. Kho, O. I. Mian and R. K. Mehra, *J. Colloid & Interface Science*, 2001, **240**, 525.
- 5 A. Di Paola, E. Garcia-López, G. Marci and L. Palmisano, *J. Hazardous Materials*, 2012, **211-212**, 3.
- 6 Y. Liu, G. Su, B. Zhang, G. Jiang and B. Yan, *Analyst*, 2011, **136**, 872.
- 7 D. Deng, S. T. Martin and S. Ramanathan, *Nanoscale*, 2010, **2**, 2685.
- 8 M. M. Khin, A. Sreekumaran Nair, V. Jagadeesh Babu, R. Murugan and S. Ramakrishna, *Energy Environ. Sci.*, 2012, **5**, 8075.
- 9 K. Ariga, S. Ishihara, H. Abe, M. Lia and J. P. Hill, *J. Mater. Chem.*, 2012, **22**, 2369.
- 10 X. B. Chen, L. Liu, P. Y. Yu and S. S. Mao, *Science*, 2011, **331**, 746.
- 11 J. Thomas, K. P. Kumar and S. Mathew, *Sci. Technol. Adv. Mater.* 2011, **3**, 59.
- 12 X. J. Xu, X. S. Fang, T. Y. Zhai, H. B. Zeng, B. D. Liu, X. Y. Hu, Y. Bando and D. Golberg, *Small*, 2011, **7**, 445.
- 13 M. A. Lazar, S. Varghese and S. S. Nair, *Catalysts*, 2012, **2**, 572.
- 14 K. Hashimoto, H. Irie and A. Fujishima, *Jap. J. Appl. Phys.* 2005, **44**, 8269.
- 15 S. M. Gupta and M. Tripathi, *Chinese Sci Bull*, 2011, **56**, 1639.
- 16 Y. Ruzmanova, M. Ustundas, M. Stoller and A. Chianese, *Chem. Eng. Transac.* 2013, **32**, 2233.
- 17 W. F. Yao, X. H. Xu, H. Wang, J. T. Zhou, X. N. Yang, Y. Zhang, S. Shang and B. B. Huang, *Appl. Catal. B: Environ.* 2004, **52**, 109.
- 18 J. Kim, D. W. Hwang, H. G. Kim, S. W. Bae, S. M. Ji, and J. S. Lee, *Chem. Commun.* 2002, **8**, 2488.
- 19 H. G. Kim, D. W. Hwang and J. S. Lee, *J. Am. Chem. Soc.* 2004, **126**, 8912.
- 20 A. Navrotsky, *Chem. Mater.* 1998, **10**, 2787.
- 21 D. M. Giaquinta and H.-C. zur Loye, *Chem. Mater.* 1994, **6**, 365.
- 22 J. M. Neil, A. Navrotsky and O. J. Kleppa, *Inorganic Chemistry*, 1971, **10**, 2076.
- 23 N. C. Wilson, J. Muscat, D. Mkhonto, P. E. Ngoepe and N. M. Harrison, *Phys. Rev. B* 2005, **71**, 075202.
- 24 N. C. Wilson, S. P. Russo, J. Muscat and N. M. Harrison, *Phys. Rev. B* 2005, **72**, 024110.
- 25 S. W. Chen, M. J. Huang, P. A. Lin, H. T. Jeng, J. M. Lee, S. C. Haw, S. A. Chen, H. J. Lin, K. T. Lu, D. P. Chen, S. X. Dou, X. L. Wang and J. M. Chen, *Appl. Phys. Lett.* 2013, **102**, 042107.
- 26 F. J. Craig, *Phys. Rev. Lett.* 2008, **100**, 167203.
- 27 P. B. Fabritichnyi, M. V. Korolenko, M. I. Afanasov, M. Danot and E. Janod, *Solid State Commun.* 2003, **125**, 341.

- 28 P. B. Fabritchnyi, A. Wattiaux, M. V. Korolenko, M. I. Afanasov and C. Delmas, *Solid State Commun.* 2009, **149**, 1535.
- 29 C. Xin, Y. Wang, Y. Sui, Y. Wang, X. Wang, K. Zhao, Z. Liu, B. Li and X. Liu, *J. Alloys & Comp.* 2014, **613**, 401.
- 30 M. Makowska-Janusik and A. Kassiba, Functional Nanostructures and Nanocomposites – Numerical Modeling Approach and Experiment, in Handbook of Computational Chemistry, Ed. J. Leszczynski, Springer 2012.
- 31 M. Makowska-Janusik, O. Gladii, A. Kassiba, J. Boucle and N. Herlin-Boime, *J. Phys. Chem. C*, 2014, **118**, 6009.
- 32 H. Melhem, P. Simon, J. Wang, C. Di Bin, B. Ratier, Y. Leconte, N. Herlin-Boime, M. Makowska-Janusik, A. Kassiba and J. Boucle, *Solar Energy Materials & Solar Cells*, 2013, **117**, 624.
- 33 P. S. Anjana and M. T. Sebastian, *J. Am. Ceram. Soc.*, 2006, **89**, 2114.
- 34 S. J. Clark, M. D. Segall, C. J. Pickard, P. J. Hasnip, M. J. Probert, K. Refson and M. C. Payne, *Z. Kristallogr.* 2005, **220**, 567.
- 35 B. G. Pfrommer, M. Cate, S. G. Louie and M. L. Cohen, *J. Comput. Phys.* 1997, **131**, 233.
- 36 J. P. Perdew, K. Burke and M. Ernzerhof, *Phys. Rev. Lett.* 1996, **77**, 3865.
- 37 J. Heyd, G. E. Scuseria, and M. Ernzerhof, *J. Chem. Phys.* 2003, **118**, 8207.
- 38 J. Heyd, G. E. Scuseria, and M. Ernzerhof, *J. Chem. Phys.* 2006, **124**, 219906.
- 39 K. Hummer, J. Harl, and G. Kresse, *Phys. Rev. B* 2009, **80**, 115205.
- 40 P. Spiewak, J. Vanhellefont, and K. J. Kurzydowski, *J. Appl. Phys.* 2011, **110**, 063534.
- 41 M. E. Foster and B. M. Wong, *J. Chem. Theory Comput.* 2012, **8**, 2682.
- 42 B. W. Wong, M. Piacenza and F. D. Sala, *Phys. Chem. Chem. Phys.* 2009, **11**, 4498.
- 43 C. O. Almbladh and A. C. Pedroza, *Phys. Rev. A* 1984, **29**, 2322.
- 44 M. Levy, J. P. Perdew and V. Sahni, *Phys. Rev. A* 1984, **30**, 2745.
- 45 A. Dreuw, J. L. Weisman and M. Head-Gordon, *J. Chem. Phys.* 2003, **119**, 2943.
- 46 M. S. Hybertsen and S. G. Louie, *Phys. Rev. B* 1986, **34**, 5390.
- 47 W. Kohn and L. J. Sham, *Phys. Rev. A* 1965, **140**, 1133.
- 48 D. C. Langreth and J. P. Perdew, *Phys. Rev. B* 1980, **21**, 5469.
- 49 P. J. Stephens, F. J. Devlin, C. F. Chabalowski and M. J. Frisch, *J. Phys. Chem.* 1994, **98**, 11623.
- 50 J. P. Perdew, M. Ernzerhof, K. Burke, *J. Chem. Phys.* 1996, **105**, 9982.
- 51 J. Heyd, G. E. Scuseria and M. Ernzerhof, *J. Chem. Phys.* 2003, **118**, 8207.
- 52 V. I. Anisimov, J. Zaanen and O. K. Andersen, *Phys. Rev. B* 1991, **44**, 943.
- 53 A. Jain, G. Hautier, S. P. Ong, C. J. Moore, C. C. Fischer, K. A. Persson and G. Ceder, *Phys. Rev. B* 2011, **84**, 045115.
- 54 R. Laskowski, N. E. Christensen, P. Blaha and B. Palanivel, *Phys. Rev. B* 2009, **79**, 165209.
- 55 Q. J. Liu and Z. T. Liu, *Appl. Phys. Lett.* 2011, **99**, 091902.
- 56 A. Sayede, R. Khenata, A. Chahed and O. Benhelal, *J. Appl. Phys.* 2013, **113**, 173501.
- 57 J. R. Huang and C. Cheng, *J. Appl. Phys.* 2013, **113**, 033912.
- 58 MOPAC2012: Stewart, J. J. P. Stewart Computational Chemistry; Colorado Springs: CO, <http://OpenMOPAC.net>.
- 59 J. J. P. Stewart, *J. Mol. Model.* 2007, **13**, 1173.
- 60 J. Baker, *J. Comput. Chem.* 1986, **7**, 385.
- 61 T. Helgaker, *Chem. Phys. Lett.* 1991, **182**, 503.
- 62 P. Culot, G. Dive, V. H. Nguyen and J. M. Ghuyssen, *J. Theor. Chim. Acta* 1992, **82**, 189.
- 63 Y. Qu, W. Zhou, Z. Ren, S. Du, X. Meng, G. Tian, K. Pan, G. Wanga and H. Fu, *J. Mater. Chem.* 2012, **22**, 16471.
- 64 R. S. Singh, T. H. Ansari, R. A. Singh and B. M. Wanklyn, *Materials Chem. & Phys.* 1995, **40**, 173.
- 65 J.-L. Wang, Y.-Q. Li, Y.-J. Byon, S.-G. Mei and G.-L. Zhang, *Powder Technology* 2013, 235, 303.
- 66 P. Salvador, C. Gutierrez, and J. B. Goodenough, *Appl. Phys. Lett.* 1982, **40**, 188.
- 67 S. Yuvaraj, V.D. Nithya, K. Saiadali Fathima, C. Sanjeeviraja, G. Kalai Selvan, S. Arumugam and R. Kalai Selvan, *Materials Research Bulletin* 2013, **48**, 1110.
- 68 T. Stein, H. Eisenberg, L. Kronik and R. Baer, *Phys. Rev. Lett.*, 2010, **105**, 266802.
- 69 R. Vijayalakshmi and V. Rajendran, *E-Journal of Chemistry*, 2012, **9**, 282.
- 70 K. P. Lopes, L. S. Cavalcante, A. Z. Simoes, J. A. Varela, E. Longo, and E. R. Leite, *J. Alloys Compd.* 2009, **468**, 327.
- 71 A. Kassiba, M. Makowska-Janusik, J. Boucle, J.F. Bardeau, A. Bulou and N. Herlin-Boime, *Phys. Rev. B* 2002, 66, 155317.
- 72 Y. Su, M.L. Balmer, *J. Phys. Chem. B* 104 (2000) 8160; G. Busca, G. Ramis, J.M. Gallardo Amcres, V. Sanchez Escribano and P. Piaggio, *J. Chem. Soc. Faraday Trans.* 1994, **90**, 3181.
- 73 F. X. Llabrés i Xamena, A. Damin, S. Bordiga and A. Zecchina, *Chem. Commun.* 2003, **13**, 1514;
- 74 M. I. Baraton, G. Busca, M. C. Prieto, G. Ricchiardi and V. Sanchez Escribano, *J. Solid State Chem.* 1994, **112**, 9.
- 75 B. A. Scott and G. Burns, *J. Am. Ceram. Soc.* 1972, 55, 225.
- 76 J. B. Bellam, M. A. Ruiz-Preciado, M. Edely, J. Szade, A. Jouanneaux, A. Kassiba, *RSC Advances*, 2015, **5**, 10551.